Superhydrophobic Fabrics Produced by Electrospinning and Chemical Vapor Deposition

Minglin Ma, Yu Mao, Malancha Gupta, Karen K. Gleason, and Gregory C. Rutledge*

Department of Chemical Engineering, Massachusetts Institute of Technology, 77 Massachusetts Avenue, Cambridge, Massachusetts 01239

Received May 31, 2005; Revised Manuscript Received August 15, 2005

ABSTRACT: A versatile method to produce superhydrophobic fabrics by combining electrospinning and initiated chemical vapor deposition (iCVD) is reported. In this study, poly(caprolactone) (PCL) was first electrospun and then coated with a thin layer of hydrophobic polymerized perfluoroalkyl ethyl methacrylate (PPFEMA) by iCVD. The hierarchical surface roughness inherent in the PCL electrospun mats and the extremely low surface free energy of the coating layer obtained by iCVD yields stable superhydrophobicity with a contact angle of 175° and a threshold sliding angle less than 2.5° for a 20 mg droplet. This PPFEMA-coated PCL mat was also shown to exhibit at least "grade 8" oleophobicity. Hydrophobicity was demonstrated to increase monotonically with a reduction in diameter among bead-free fibers and with the introduction of a high density of relatively small diameter beads. The systematic effect of fiber morphology on superhydrophobicity was also investigated theoretically and experimentally using both beaded and bead-free fibers with diameters ranging from 600 to 2200 nm.

Introduction

Superhydrophobic surfaces with water contact angles higher than 150° have drawn great scientific and industrial interest due to their applications involving water repellency, self-cleaning, and antifouling properties.[1−5] Generally, both the surface chemistry and the surface roughness affect hydrophobicity.[6,7] For a flat solid surface, the contact angle θ can be described by Young's equation,[8] $\cos\theta = (\gamma_{SV} - \gamma_{SL})/\gamma_{LV}$, where γ_{ij} is the surface tension of the solid−vapor, solid−liquid, and liquid−vapor interfaces, respectively. However, because of the limitations of interfacial tension, surface chemistry alone is insufficient to achieve superhydrophobicity. A superhydrophobic surface requires in addition a certain surface roughness whose effect on the apparent contact angle θ^* was studied decades ago by Wenzel,[9,10] Cassie and Baxter,[11] and Johnson and Dettre.[12,13] In the Wenzel hydrophobic state, the water droplet penetrates into the surface cavities and remains pinned to the surface, which magnifies the wetting property of the surface and leads to a high hysteresis (the difference between the advancing and the receding contact angles) or a high threshold sliding angle. In this state, the surface roughness r, defined as the ratio of the actual contact area to the apparent surface area, is used to relate θ^* and θ as $\cos\theta^* = r\cos\theta$. In the Cassie−Baxter state, the liquid does not follow the surface contours but instead bridges across the surface protrusions and sits upon a composite surface composed of both solid and air patches; in this case, the apparent liquid contact angle is described by $\cos\theta^* = \phi_s\cos\theta - \phi_v$, where ϕ_s and ϕ_v are the solid−liquid and gas−liquid contact area per unit projected surface area, respectively. The Cassie−Baxter state also has a low hysteresis and threshold sliding angle because the water can slide or roll easily when it sits partly on air; therefore, in real applications, the stable Cassie−Baxter state is generally more desirable for applications where water needs to be shed. Based on these principles, numerous methods have been reported to produce superhydrophobic surfaces by either increasing the surface roughness of an inherently hydrophobic material[14−16] or decreasing the surface free energy of a rough surface by posttreatment.[17−20]

Electrospinning is a simple but versatile method to produce continuous, submicron diameter fibers. It has recently been shown to provide the appropriate surface roughness to make superhydrophobic surfaces.[21−23] Both experimental[24−28] and theoretical studies[29−34] have been conducted to characterize the process and control the fiber morphology. These studies clearly show that the formation of ultrathin fibers is achieved by the stretching of the polymer jet associated with the onset of a whipping instability caused by the electrostatic forces. The polymeric fluid must have adequate viscoelasticity (usually controlled by an appropriate combination of molecular weight and concentration of the polymer in solution) and conductivity in order to be electrospinnable, i.e., to form uniform fibers. Otherwise, the surface tension, which tends to break the liquid jet into droplets (the effect known as Rayleigh instability), dominates the process, and beaded fibers or polymeric microdroplets will be formed instead of uniform fibers. The diversity of electrospinnable materials and the interesting properties of electrospun fibers have led to applications ranging from composite materials, sensing technology, and filtration to tissue engineering and biomedical applications.[35−39]

Initiated chemical vapor deposition (iCVD) is a one-step, solvent-free deposition technique. The conformal nature of the iCVD process enables coating on complex substrates. It allows films of nanoscale thicknesses to be produced and has been used to coat nanoscale features.[18] Fluoropolymer coatings are well-known for their low surface energies, with poly(tetrafluoroethylene) (PTFE, $(-CF_2-)_n$) having $\gamma_s \sim 20$ mN/m[40] and fluorinated acrylic polymers exhibiting even lower values of γ_s (5.6−7.8 mN/m) due to their CF_3-terminated

* Corresponding author: e-mail rutledge@mit.edu; Tel (617) 253−0171; Fax (617) 258-8992.

10.1021/ma0511189 CCC: $30.25
Published on Web 10/14/2005

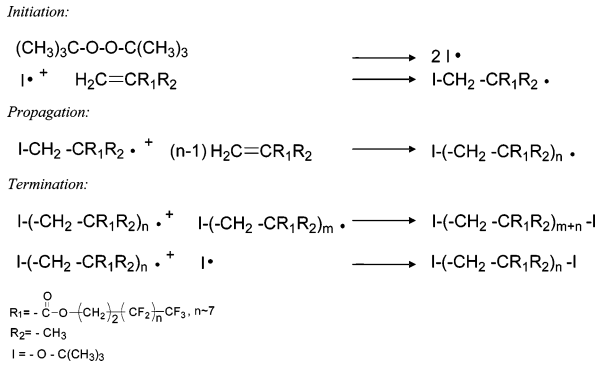

Figure 1. Reaction mechanism for PPFEMA iCVD with *tert*-butyl peroxide as an initiator.

side chains and their comblike structure.[41,42] The iCVD technique has been successfully applied in polymerizing perfluoroalkyl ethyl methacrylate (PFEMA, $CH_2{=}C(CH_3)$-$COOCH_2CH_2(CF_2)_nCF_3$, $n \sim 7$, Zonyl) using *tert*-butyl peroxide as an initiator.[43] The dispersive surface energy of the resulting poly(PFEMA) (PPFEMA) coating is 9.3 mN/m. The process involves thermal decomposition of the initiator molecule into free radical species and subsequent addition reaction of the monomer, as shown in Figure 1.

In previous work,[23] a superhydrophobic surface in the form of nonwoven textiles was achieved in a single process step by electrospinning a hydrophobic material. In this paper we develop a method to make even more highly superhydrophobic fabrics by combining electrospinning and iCVD. The broad range of materials that can be electrospun, combined with the benign and conformal nature of the iCVD coating, makes this method quite versatile. In principle, any electrospinnable material, including those that may dissolve or decompose upon exposure to certain solvents or high temperatures, can be used. PCL is selected for a demonstration here because of the ease with which fibers can be formed over a range of diameters,[34] which in turn permits a more detailed study of the role of fiber morphology on hydrophobicity. PCL is well-known for its biodegradability and has been electrospun into fiber mats for use as scaffolds in tissue engineering.[44,45] The morphology of PCL fibers can be simply tailored by varying the solution concentration and operating parameters during electrospinning.[34,46] In the subsequent iCVD process, a fluoroacrylate, PFEMA, is polymerized to coat the electrospun mats. Contact angle measurements reveal that all the poly(perfluoroalkyl ethyl methacrylate) (PPFEMA) modified PCL samples studied in this work exhibit superhydrophobicity. On one hand, the hierarchical structure of the electrospun mat, comprising nanoscale fibers and micron-scale beads and interfibrillar distances, dramatically increases the surface roughness and the fraction of contact area of water with the air trapped in the apertures among fibers; on the other hand, the thin layer of PPFEMA coating prevents the water from sinking into the cavities and pinning to the surface. The combination of these two effects is believed to lead to the superhydrophobicity of the iCVD-coated electrospun mats. We further study the effect of fiber morphology on the hydrophobicity and find that thin fibers having a high density of beads are more hydrophobic than thicker, bead-free fibers.

Experimental Section

PCL (Aldrich) with a weight-averaged molecular weight M_w = 80K was used in this study. A series of PCL solutions of different concentrations were made with a mixture of chloroform (Aldrich) and methanol (Aldrich) (3/1 by weight) as the solvent. The solutions were electrospun using a parallel plate setup to provide a uniform electric field and to avoid corona discharge at high voltages, as described previously.[26] The concentrations and operating parameters are summarized in Table 1.

The fiber morphologies were observed by a JEOL-6060SEM (JEOL Ltd., Japan) scanning electron microscope (SEM). The fibers were sputter-coated with a 2−3 nm layer of gold for imaging using a Desk II cold sputter/etch unit (Denton Vacuum LLC, Moorestown, NJ). The fiber diameters and bead sizes were determined using AnalySIS image processing software (Soft Imaging System Corp., Lakewood, CO).

PPFEMA films were deposited onto PCL mats in a custom-built 200 mm diameter reactor described elsewhere.[47] The reactor was equipped with a stainless steel filament array, which was heated resistively to 250 °C to decompose the initiator thermally to form free radicals, and a water-cooled stage (35 °C) on which the substrate was placed. Pressure in the vacuum chamber was maintained at 0.3 Torr. *tert*-Butyl peroxide (Aldrich) was used as the initiator and vaporized at room temperature. The PFEMA monomer (Aldrich) was vaporized in a glass jar that was heated to 90 °C. The flow rates of peroxide and PFEMA were regulated using needle valves and kept constant at 0.1 and 0.8 sccm, respectively. For each deposition, a silicon wafer was placed close to the PCL mat as a reference for film growth and was monitored in-situ using an interferometry system equipped with a 632.8 nm HeNe laser source. Film thicknesses on the wafer substrates were measured using profilometry (Tencor P10) and ranged from 70 to 100 nm.

A Kratos Axis Ultra X-ray photoelectron spectrometer (XPS) (Kratos Analytical, Manchester) with a monochromatized Al Kα X-ray source was used to analyze the surface chemistry of the as-spun mats and coated mats.

The contact angles of water on the mats were measured using a contact angle meter G10 (Kruss, Germany). The final result for each sample was obtained by averaging at least four separate runs. The threshold sliding angles were determined by first placing a 20 mg droplet gently on a level surface (tilt stage, THORLABS) and then slowly tilting the surface until the droplet starts moving.

Results and Discussion

PCL mats with different fiber morphologies, including beaded fibers and bead-free fibers as well as variations in fiber diameter, were obtained by varying the concentrations and operating parameters during electrospinning (see Table 1). Selected SEM images are shown in Figure 2. As the label index increases, the average fiber diameter decreases for both the bead-free and beaded fibers as quantified in Table 1. For beaded fibers, the average diameter refers to the diameter of the threads between the beads. Additionally, the bead size decreases and the bead density increases with increasing label index of the beaded samples. The areal bead density can be defined as the number of beads per unit area, while a linear bead density can be defined as the number of beads per unit length of fiber. However, both of these are difficult to quantify in a meaningful way since the areal bead density depends also on the thickness of the mat and the density of fibers therein, while the linear bead density requires an analysis of the total linear length of fibers as well as a count of the number of beads present in a sample of material. Here we characterize the bead density only in a qualitative sense (i.e., through visualization) under the assumption that mat thickness

Table 1. Solution Concentrations, Operating Parameters, and Average Fiber Diameter and Bead Size of PCL Electrospun Mats

sample index[a]	concn (wt %)	flow rate (mL/min)	voltage (kV)	plate-to-plate distance (cm)	fiber morphology	
					av fiber diameter (nm)	av bead size (nm)
F1	11.5	0.05	37.6	27	2200	no bead
F2	10.0	0.05	35.0	27	2000	no bead
F3	9.2	0.025	32.5	27	1900	no bead
F4	7.6	0.025	18.6	40	1400	no bead
F5	7.1	0.025	25.9	40	620	no bead
F6	7.1	0.025	35.0	27	580	no bead
B1	6.4	0.05	33.0	27	590	7350
B2	6.7	0.025	23.1	40	320	6760
B3	5.2	0.025	22.5	40	210	5880
B4	4.0	0.05	25.4	45	180	3530
B5	2.0	0.05	25.4	45	110	2650

[a] Sample labels starting with "F" are bead-free fibers while those starting with "B" are beaded fibers.

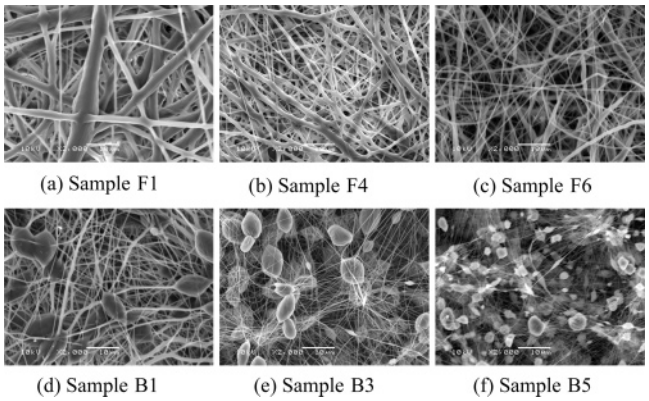

Figure 2. Typical SEM images of the PCL electrospun mats. Scale bars = 10 μm.

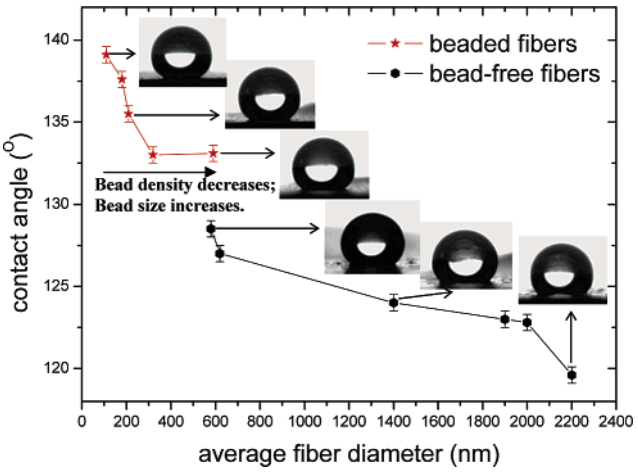

Figure 3. Contact angles for the as-spun PCL mats. From bottom to top in the inset are representative droplet images on samples F1, F4, F6, B1, B3, and B5. The contact angles are 119°, 124°, 129°, 133°, 135°, and 139°, respectively. The error bars are indicative of statistical variations among multiple measurements; other sources of uncertainty, such as image quality, curve-fitting procedures, and operator estimation, suggest that the uncertainty in contact angle determination could be as large as ±3°.

and fiber density are qualitatively similar for all mats. The transition here from bead-free fibers to beaded fibers is believed to be a result of the late onset of nonlinear viscoelastic effects during growth of a Rayleigh instability in the whipping portion of the jet.[24,29,48]

We first studied the hydrophobicity of the as-spun PCL mats. Figure 3 shows how the initial contact angle (measured within 1 min of placement of the drop on the mat) varies with average fiber diameter. Selected droplet images are shown in the inset. Since the PCL is not a hydrophobic material (PCL solution cast film shows a contact angle of 60°), the initial hydrophobicity of the as-spun mats is metastable: the contact angle decreases gradually with time over a period of about 20 min under ambient conditions. The origin of this decrease in contact angle is believed to be due to two effects. The first is the evaporation of water from the droplet, which changes the contact angle from advancing to receding. The second is conversion of the contact zone from an initial Cassie−Baxter state to a final Wenzel state as the water droplet sinks into the interstices of the mat. Significantly, Wenzel's equation predicts a lower apparent contact angle for a rough surface if the material is not hydrophobic (i.e., Young's contact angle is less than 90°). The formation initially of a Cassie−Baxter state, wherein the droplet sits on a heterogeneous surface of fiber and air, could be a consequence of trapping the air when the droplet is first placed gently on such a fibrous mat. The metastable nature of the Cassie−Baxter state in this case can also be demonstrated by applying pressure to the droplet[2,22] or by allowing the droplet to fall freely from an elevated height to contact with the mat. Dropping the beads of water onto the mat from a height of 8 cm, we observed contact angles for these same as-spun mats as low as 10°. This metastable nature of the hydrophobic state is further verified by the fact that the droplet does not slide even when the mat is tilted to 90° due to the pinning effect. Nevertheless, the initial contact angles still provide useful information on surface roughness. Namely, as shown in Figure 3, the contact angles for both beaded fibers and bead-free fibers increase as the average fiber diameter decreases. The contact angles for the beaded fibers increase as the bead density increases and the bead size decreases. Therefore, we conclude that the thinner, beaded fibers have higher surface roughness and therefore higher initial contact angles than the thicker, bead-free fibers.

To obtain a stable superhydrophobicity for these electrospun PCL mats, surface modification through iCVD coating is employed. A thin and conformal iCVD coating can dramatically decrease the surface energy while maintaining the inherent surface roughness of the electrospun mats. Figure 4a,b shows representative SEM images of a PCL mat (sample B1) before and after coating. The thickness of the PPFEMA coating is difficult to determine directly on the fibers; however, a coating thickness of 70 nm was measured on a reference silicon wafer. The thickness is anticipated to be smaller for the coating on the fibers due to the high surface area

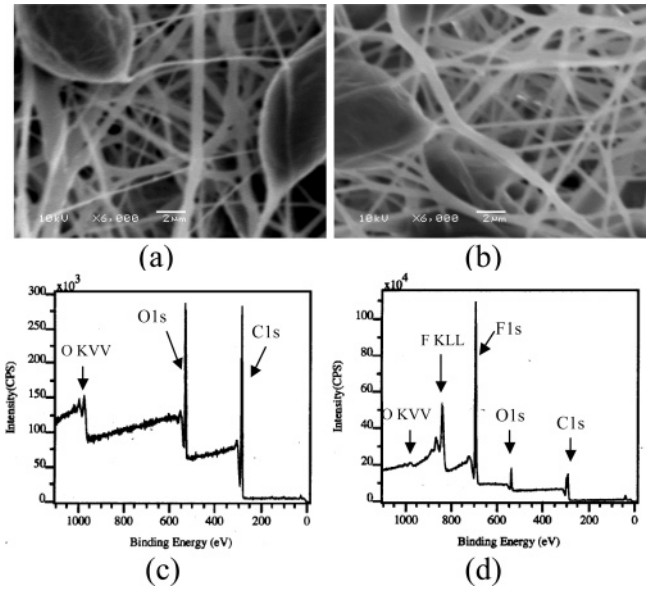

Figure 4. SEM images of sample B1 (a) before and (b) after iCVD coating (scale bars = 2 μm); (c) and (d) are corresponding XPS data for (a) and (b), respectively.

of the electrospun mats. The conformal nature of the iCVD process results in little overall change in the hierarchical nature of the mat morphology, the only visually observable change being the slight increase in fiber diameter.

XPS scans were used to verify further the presence of PPFEMA on the coated mats. Figure 4c,d shows the XPS scans of an as-spun PCL mat (sample B1) and the same mat coated with PPFEMA. Figure 4d shows that the PPFEMA-coated mat contains a strong peak in the 690−700 eV region. This peak is characteristic of fluorine 1s and indicates the presence of PPFEMA on these substrates. The XPS scan of the uncoated mat in Figure 4c confirms that it does not contain any characteristic fluorine peaks, as expected.

The contact angles for water on all the PPFEMA-coated PCL mats are summarized in Figure 5, with selected droplet images shown in the inset. The highest contact angle for the PPFEMA coated mats is larger than 175°. In Figure 5, thinner, beaded fibers are observed to give mats with higher contact angles than thicker, bead-free fibers, which is in good agreement with the trend for the as-spun mats. Specifically, for bead-free fibers, mats with smaller fibers are more hydrophobic than those with larger fibers; for beaded fibers, a high density of smaller beads imparts higher hydrophobicity than a low density of larger beads. Last, for the same fiber diameters, the mats with beaded fibers are more hydrophobic than those composed of bead-free fibers. In contrast to the metastable hydrophobicity of the as-spun PCL mats, the superhydrophobicity of the PPFEMA coated mats is stable; a free falling droplet bounces off the surface and splits into smaller droplets instead of spreading on the mat and penetrating into the interstices, as in the case of as-spun mats.

To understand better the effect of fiber morphology on the superhydrophobicity, theoretical studies were performed, based on the Cassie−Baxter equation.[11] For the sake of simplicity, we use parallel cylinders to represent bead-free fibers and square-packed spheres to represent the beads on the fibers (see Figure 6). Figure 6a shows cross-sectional and top-down views of

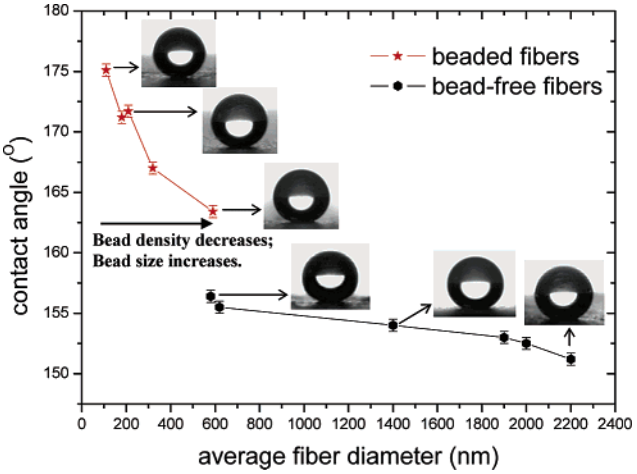

Figure 5. Contact angles for PPFEMA-coated PCL mats. From right to left in the inset are representative droplet images on samples F1, F4, F6, B1, B3, and B5. The corresponding contact angles are 151°, 154°, 156°, 163°, 172°, and 175°, respectively. The error bars are indicative of statistical variations among multiple measurements; other sources of uncertainty, such as image quality, curve-fitting procedures, and operator estimation, suggest that the uncertainty in contact angle determination could be as large as ±3°.

the water droplet sitting across the fibers, where the bending of the water−fiber interface and the contact area is determined by the intrinsic contact angle, θ, as shown in the figure. Figure 6b shows cross-sectional and top-down views of the droplet sitting on the tops of beads, where the wetted area enclosed by the dash lines is determined again by the intrinsic contact angle. We have assumed the water can be described by the Cassie−Baxter state and thus does not penetrate into the apertures of the mat. This is a valid assumption for the mats employed in this work because the hydrostatic pressure which must be overcome in order for penetration to occur is much larger than atmospheric pressure for micrometer-sized apertures.[49] The contact angle, θ, for PPFEMA is 119°, obtained by measuring the contact angle on the PPFEMA-coated silicon wafer. From this, we calculate the apparent contact angle, θ^*, as a function of $x = d/s$, the ratio of diameter (cylinder or sphere) to separation distance, using the following equations:

$$\cos\theta^* = \frac{x(\pi - \theta)}{x+1}\cos\theta + \frac{x\sin\theta}{x+1} - 1$$

for the case of cylinders and

$$\cos\theta^* = \frac{\pi x^2(1+\cos\theta)}{2(x+1)^2}\cos\theta + \frac{\pi x^2\sin^2\theta}{4(x+1)^2} - 1$$

for the case of spheres. Figure 6c shows how these theoretical apparent contact angles for PPFEMA-coated cylinders and spheres vary with d/s. The contact angle decreases as the diameter increases if the separation distance is fixed. Figure 6c also shows that the droplet sitting on spheres has a higher contact angle than that sitting on cylinders of comparable radius. Both of the predictions are consistent with the experimental data. No attempt is made here to fit the data precisely since the random orientation of fibers in the real materials, as well as the three-dimensional nature of the mats imaged, for example, in Figure 2, complicates the

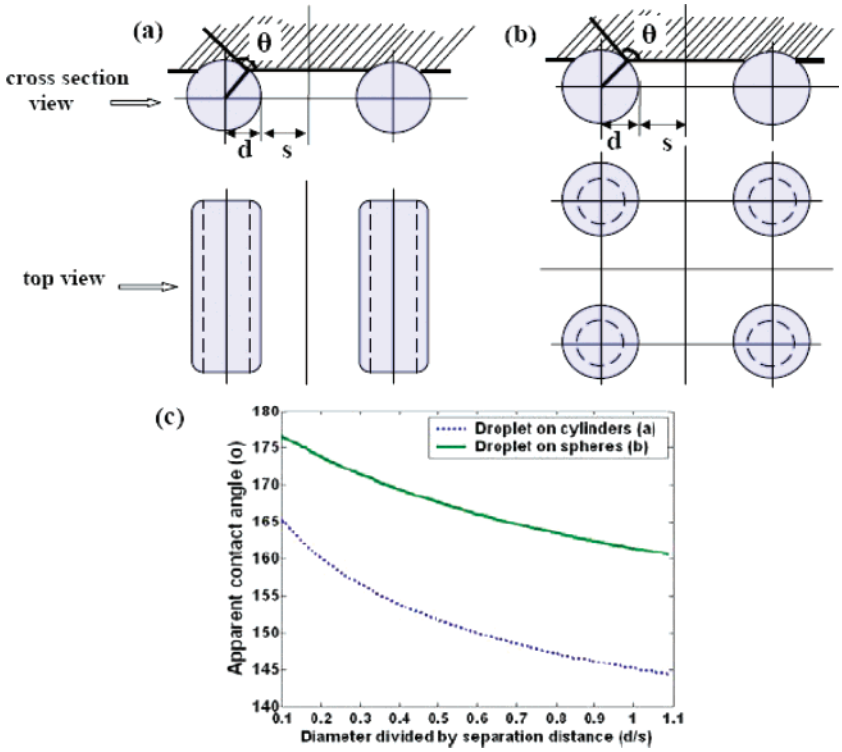

Figure 6. Schematic representations of water droplet sitting on (a) cylinders and (b) spheres. The shaded area represents water and the dashed lines represent triphasic contact lines. (c) Corresponding apparent contact angles for (a) and (b).

determination of an appropriate value for the separation distance between fibers. For beaded fibers, the assumption that the droplet only sits on beads might also break down if the areal bead density is so low that the normal component of surface tension is not sufficient to suspend the droplet only on beads (e.g., see sample B1). At this point, we hypothesize that if the water sits on both fibers and beads, the contact angle values should fall between the two curves depicted in Figure 6c. Nevertheless, the simplified model provides useful ranges of contact angles for both bead-free fibers and beaded fibers, and all the experimental contact angles roughly fall in these ranges.

It has been suggested that a useful water-repellent surface should have not only a high static contact angle but also a low contact angle hysteresis or threshold sliding angle.[1,2] Both the hysteresis and sliding angle are important parameters to determine the sliding resistance. Figure 7 shows the threshold sliding angles of a 20 mg droplet on the PPFEMA-coated PCL mats with different fiber morphologies. The sliding angle is observed to decrease concurrent with the increase in superhydrophobicity from sample F1 to F6 and from B1 to B5, confirming the conclusion we made previously from the static contact angle measurements. All the sliding angles shown in Figure 7 are less than 12°, again in direct contrast to the as-spun mats, where the droplet does not slide even when the surface is tilted to 90°. The lowest sliding angle is 2.5°, observed for sample B5, which also has the highest static contact angle at 175°.

The surface energies of these PPFEMA-coated PCL mats are low enough to result in oleophobicity. Oleophobicity has received much less attention[50,51] but is often more desirable than simple superhydrophobicity and is generally more difficult to achieve. Oleophobicity together with superhydrophobicity can significantly enhance the self-cleaning ability of a surface, especially the resistance to organic contamination. Oleophobicity

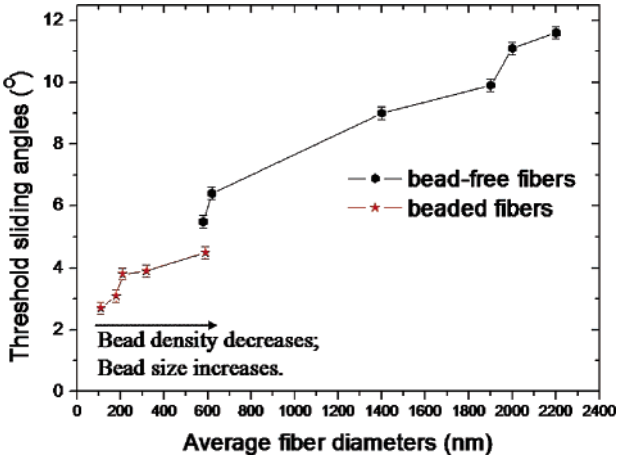

Figure 7. Threshold sliding angles for the PPFEMA-coated PCL mats.

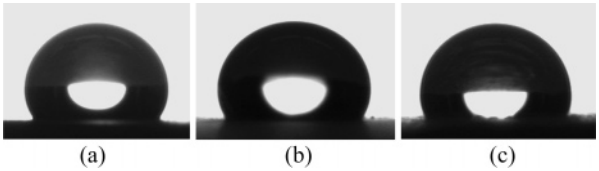

Figure 8. Alkane droplets on the PPFEMA-coated sample F1: (a) *n*-decane, (b) *n*-octane, and (c) *n*-heptane. The contact angles are 118°, 109°, and 92°, respectively.

of the PPFEMA-modified PCL mats was measured using the AATCC (American Association of Textile Chemists and Colorists) test method 118-1997,[52] in which the material is challenged with a series of test liquids, including *n*-decane, *n*-octane, and *n*-heptane. The contact angles (see Figure 8) of these three alkanes on the PPFEMA-coated sample F1 are 118°, 109°, and 92°, respectively, which are much larger than those on the PPFEMA-coated Si wafer (53°, 45°, and 32°, respec-

tively), indicating at least a grade 8 (*n*-heptane-phobic) oil repellency. Since the intrinsic contact angle for *n*-heptane on the a smooth PPFEMA film is less than 90°, the apparent contact angles on a rough PPFEMA surface should be even lower, according to the Wenzel equation. From this, we conclude that the contact angles shown in Figure 8 are metastable, similar to the case for water on as-spun PCL mats. The 5 mg droplets of *n*-decane, *n*-octane, and *n*-heptane at ambient temperature in stagnant air exhibit contact angles lower than 90° in periods of about 39, 6, and 1 min, respectively. We anticipate that these times would also depend on the alkane evaporation rate, which includes factors such as temperature, air velocity, and droplet size.

Conclusion

The fabrication of superhydrophobic nonwoven fabrics through a two-stage process of electrospinning to generate surface roughness, followed by initiated chemical vapor deposition to reduce surface energy, is demonstrated here. This two-stage process allows a decoupling of the constraints on fiber composition and electrospinning technology, used to control the morphology and roughness of the nonwoven fabric, from that of the surface-active hydrophobic layer chemistry required to maximize hydrophobicity. PCL was selected as an example to demonstrate the concept because of the ease of control over surface roughness it allows during electrospinning, but the composition of the electrospun substrate is relatively unimportant to the final superhydrophobicity of the material due to the use of a subsequent iCVD surface coating step that provides the desired surface chemistry. The selection of composition for the electrospun fiber substrate can therefore be based on other performance criteria, such as toughness, thermal stability, or weight. The extremely low surface energy of the PPFEMA coating material and the high surface roughness inherent in the electrospun mats produce stable superhydrophobic nonwoven mats with contact angles as high as 175°, from which water rolls off freely. These PPFEMA-coated electrospun mats also show a high oleophobicity with a grade 8 oil repellency. This study also suggests that thinner, beaded fibers are more favorable than thicker, bead-free fibers in terms of hydrophobicity. We expect that the method introduced here can be applied to virtually any electrospinnable and compatible substrate to develop superhydrophobic fabrics.

Acknowledgment. This research was supported in part by the U.S. Army through the Institute for Soldier Nanotechnologies, under Contract DAAD-19-02-D-0002, with the U.S. Army Research Office. The content does not necessarily reflect the position of the Government, and no official endorsement should be inferred. We are grateful to Dr. Randal M. Hill of Dow Corning and Mr. Jian H. Yu of MIT for their helpful discussions and assistance during this project and also to Mr. Brad Cicciarelli of MIT for the contact angle measurements.

References and Notes

(1) Feng, L.; Li, S.; Li, Y.; Li, H.; Zhang, L.; Zhai, J.; Song, Y.; Liu, B.; Jiang, L.; Zhu, D. *Adv. Mater.* **2002**, *14*, 1857.
(2) Quéré, D. *Nat. Mater.* **2002**, *1*, 14.
(3) Lafuma, A.; Quéré, D. *Nat. Mater.* **2003**, *2*, 457.
(4) Blossey, R. *Nat. Mater.* **2003**, *2*, 301.
(5) Erbil, H. Y.; Demirel, A. L.; Avcı, Y.; Mert, O. *Science* **2003**, *299*, 1377.
(6) Nakajima, A.; Hashimoto, K.; Watanabe, T. *Monatsh. Chem.* **2001**, *132*, 31.
(7) Quéré, D. *Physica A* **2002**, *313*, 32.
(8) Young, T. *Philos. Trans. R. Soc. London* **1805**, *95*, 65.
(9) Wenzel, R. N. *Ind. Eng. Chem.* **1936**, *28*, 988.
(10) Wenzel, R. N. *J. Phys. Colloid Chem.* **1949**, *53*, 1466.
(11) Cassie, A. B. D.; Baxter, S. *Trans. Faraday Soc.* **1944**, *40*, 546.
(12) Johnson, R. E.; Dettre, R. H. *Adv. Chem. Ser.* **1964**, *43*, 112.
(13) Johnson, R. E.; Dettre, R. H. *Adv. Chem. Ser.* **1964**, *43*, 136.
(14) Onda, T.; Shibuichi, S.; Satoh, N.; Tsujii, K. *Langmuir* **1996**, *12*, 2125.
(15) Feng, L.; Li, S.; Li, H.; Zhai, J.; Song, Y.; Jiang, L.; Zhu, D. *Angew. Chem., Int. Ed.* **2002**, *41*, 1221.
(16) Quéré, D.; Lafuma, A.; Bico, J. *Nanotechnology* **2003**, *14*, 1109.
(17) Yoshimitsu, Z.; Nakajima, A.; Watanabe, T.; Hashimoto, K. *Langmuir* **2002**, *18*, 5818.
(18) Lau, K. K. S.; Bico, J.; Teo, K. B. K.; Chhowalla, M.; Amaratunga, G. A. J.; Milne, W. I.; McKinley, G. H.; Gleason, K. K. *Nano Lett.* **2003**, *3*, 1701.
(19) Woodward, I.; Schofield, W. C. E.; Roucoules, V.; Badyal, J. P. S. *Langmuir* **2003**, *19*, 3432.
(20) Zhai, L.; Cebeci, F. C.; Cohen, R. E.; Rubner, M. F. *Nano Lett.* **2004**, *4*, 1349.
(21) Jiang, L.; Zhao, Y.; Zhai, J. *Angew. Chem., Int. Ed.* **2004**, *43*, 4338.
(22) Acatay, K.; Simsek, E.; Ow-Yang, C.; Menceloglu, Y. Z. *Angew. Chem., Int. Ed.* **2004**, *43*, 5210.
(23) Ma, M.; Hill, R. M.; Lowery, J. L.; Fridrikh, S. V.; Rutledge, G. C. *Langmuir* **2005**, *21*, 5549.
(24) Fong, H.; Chun, I.; Reneker, D. H. *Polymer* **1999**, *40*, 4585.
(25) Reneker, D. H.; Yarin, A. L.; Fong, H.; Koombhongse, S. *J. Appl. Phys.* **2000**, *87*, 4531.
(26) Shin, Y. M.; Hohman, M. M.; Brenner, M. P.; Rutledge, G. C. *Polymer* **2001**, *42*, 9955.
(27) Shin, Y. M.; Hohman, M. M.; Brenner, M. P.; Rutledge, G. C. *Appl. Phys. Lett.* **2001**, *78*, 1149.
(28) Theron, S. A.; Zussman, E.; Yarin, A. L. *Polymer* **2004**, *45*, 2017.
(29) Yarin, A. L.; Koombhongse, S.; Reneker, D. H. *J. Appl. Phys.* **2001**, *89*, 3018.
(30) Yarin, A. L.; Koombhongse, S.; Reneker, D. H. *J. Appl. Phys.* **2001**, *90*, 4836.
(31) Hohman, M. M.; Shin, Y. M.; Rutledge, G. C.; Brenner, M. P. *Phys. Fluids* **2001**, *13*, 2201.
(32) Hohman, M. M.; Shin, Y. M.; Rutledge, G. C.; Brenner, M. P. *Phys. Fluids* **2001**, *13*, 2221.
(33) Feng, J. J. *Phys. Fluids* **2002**, *14*, 3912.
(34) Fridrikh, S. V.; Yu, J. H.; Brenner, M. P.; Rutledge, G. C. *Phys. Rev. Lett.* **2003**, *90*, 144502.
(35) Frenot, A.; Chronakis, I. S. *Curr. Opin. Colloid Interface Sci.* **2003**, *8*, 64.
(36) Huang, Z.-M.; Zhang, Y.-Z.; Kotaki, M.; Ramakrishna, S. *Compos. Sci. Technol.* **2003**, *63*, 2223.
(37) Li, D.; Xia, Y. *Adv. Mater.* **2004**, *16*, 1151.
(38) Dzenis, Y. *Science* **2004**, *304*, 1917.
(39) Thandavamoorthy, S.; Bhat, G. S.; Tock, R. W.; Parameswaran, S.; Ramkumar, S. S. *J. Appl. Polym. Sci.* **2005**, *96,* 557.
(40) Thunemann, A. F.; Lieske, A.; Paulke, B. R. *Adv. Mater.* **1999**, *11*, 321.
(41) Anton, D. *Adv. Mater.* **1998**, *10*, 1197.
(42) Tsibouklis, J.; Nevell, T. G. *Adv. Mater.* **2003**, *15*, 647.
(43) Mao, Y.; Gleason, K. K. *Langmuir* **2004**, *20*, 2484.
(44) Yoshimoto, H.; Shin, Y. M.; Terai, H.; Vacanti, J. P. *Biomaterials* **2003**, *24*, 2077.
(45) Li, W.-J.; Tuli, R.; Okafor, C.; Derfoul, A.; Danielson, K. G.; Hall, D. J.; Tuan, R. S. *Biomaterials* **2005**, *26*, 599.
(46) Lee, K. H.; Kim, H. Y.; Khil, M. S.; Ra, Y. M.; Lee, D. R. *Polymer* **2003**, *44*, 1287.
(47) Chan, K.; Gleason, K. K. *Langmuir* **2005**, *21*, 8930.
(48) McKee, M. G.; Wilkes, G. L.; Colby, R. H.; Long, T. E. *Macromolecules* **2004**, *37,* 1760.

(49) Youngblood, J. P.; McCarthy, T. J. *Macromolecules* **1999**, *32*, 6800.
(50) Chen, W.; Fadeev, A. Y.; Hsieh, M. C.; Oner, D.; Youngblood, J.; McCarthy, T. J. *Langmuir* **1999**, *15*, 3395.
(51) Yabu, H.; Takebayashi, M.; Tanaka, M.; Shimomura, M. *Langmuir* **2005**, *21*, 3235.
(52) AATCC test method 118-1997 scale (AATCC Technical Manual American Association of Textile Chemists and Colorists, Research Triangle Park, NC, 1996, http://www.aatcc.org/Technical/Test_Methods/Alpha_List.htm).

MA0511189